Spray Characteristics and Vaporization process of ammonia-ethanol blends with a current Bosch GDI engine injector

Ronan Pelé, Pierre Brequigny, Camille Hespel, Jérôme Bellettre, Christine Mounaïm-Rousselle

Spray Characteristics and Vaporization process of ammonia-ethanol blends with a current Bosch GDI engine injector

R. Pelé*[1], P. Bréquigny[1], C. Hespel[1], J. Bellettre[2], C. Mounaïm-Rousselle[1]
[1]Univ. Orléans, INSA-CVL, EA 4229 – PRISME, F-45072 Orléans, France
[2]Laboratoire de Thermique et Energie de Nantes (LTeN UMR Université de Nantes—CNRS 6607)
*Corresponding author: ronan.pele@etu.univ-orleans.fr

Abstract
The study aims to provide information on the spray characteristics and vaporization process of ammonia-ethanol blends with a current GDI injector at different air densities and temperatures. The Schlieren technique was used to capture images of liquid spray. The penetration length and the spray angle at quarter-penetration length were measured and are clearly dependent on the ammonia ratio at low pressure, around 2 bar. A part of this study focuses on the vaporization process of the different blends with a comparison of the modeling of one single droplet vaporization. The calculation indicated a droplet temperature drop: from 9°C to -63°C from pure ethanol to pure ammonia, respectively.

Introduction
Using carbon-free energy sources is one of the keys to mitigating climate change. Ammonia is one interesting molecule for efficient and safe hydrogen storage (17.8% by weight) in the liquid phase at approximately 9 bar at 20°C or −34 °C at ambient pressure. Moreover, it is also more and more considered as a zero-carbon fuel for thermal engines or gas turbines. However, its high auto-ignition temperature and research octane number, narrow flammability range, and low laminar flame speed [1] are unfavorable combustion properties. Blending ammonia with more reactive fuels is one solution to improve combustion properties.

Several studies have addressed the potential of ammonia blended with another fuel in internal combustion engines to promote ignition/combustion properties, as reviewed in Mounaïm-Rousselle and Brequigny [2] and Dimitriou and Javaid [3]. Biofuels, and particularly bio-ethanol, are also another interesting alternative energy sources to contribute to the decarbonization of the transportation sector [4]. Even if the potential of blending ethanol into ammonia is promising due to the perfect solubility between both liquids [6-8], no data are available on the injection process for this kind of blend. Indeed, the injection process is a fundamental aspect especially for internal combustion engine optimization as it allows the control of the in-cylinder air-to-fuel ratio and affects the pollutant emission itself [5]. The advantage of direct injection compared to port-fuel is to vaporize as fast as possible the fuel inside the chamber by breaking up the fuel spray into droplets. Then, the vaporization of droplets is greatly significant for the spatial distribution of fuel vapor/air, the ignition, and the combustion itself. Generally, the use of high-pressure injection systems [6] favors the atomization in small droplets which enhances the liquid-air interface, the vaporization, and the fuel/air mixing [7,8]. The effects of injection pressure on droplet size reduction become limited or even disappear when the injection pressure reaches a threshold [6]. Another possibility to reduce droplet size is the flash boiling condition itself, which produces finer droplets and a more uniform fuel/air mixture [6]. Flash boiling is a thermodynamic state of fuel spray that occurs when a subcooled liquid is rapidly depressurized to a pressure below its liquid saturation pressure [9].

Adding ethanol into ammonia generates an “effervescent-like” atomization due to their high difference in vapor pressures : $P^{Sat}_{C_2H_5OH}(293K) = 5.4kPa$ and $P^{Sat}_{NH_3}(293K) = 855.8kPa$, [10][11] thus potentially improving the ethanol vaporization when the pressure is below the saturation pressure of ammonia during the direct injection.

Therefore, the objective of the present experimental study is to investigate the spray characteristics of ammonia/ethanol blends under different ammonia ratios (25%, 50%, 75%, and 90% of mole fraction of ammonia), at different air densities and temperatures in a constant-volume chamber at 120 bar of injection pressure. The Schlieren optical technique was used to capture images of liquid spray. The penetration length and the spray angle at quarter-penetration length were measured. The second part of this work focuses on the vaporization process of the different blends at different conditions of air density and temperature. The modeling of one single droplet vaporization is studied in order to complete the understanding of the vaporization process.

Material and methods

A constant volume 2.5 L chamber was used to follow the spray development. As described in [12], it can be pressurized to the desired pressure up to 30 bar by an air compressor and warmed up to 200 °C by wall heating resistances. Between each spray, the chamber is purged with flushed air that is vented to the outside. All the different blends are pressurized up to 120 bar by pressurized Helium. A current gasoline direct Bosch injector (7 holes of 150 µm diameter and its reference number is 0261500494) is used to generate the spray. The temperature and injection duration are controlled through an automation system driven by a Labview program. The pressure and the temperature are measured by a pressure sensor from KELLER (PAA-33X model) and a T thermocouple with a precision of ±4 mbar and ±0.1 K respectively.

Schlieren Setup

The Schlieren technique, based on the measurement of the deviation of the light source through the test section, was used to follow the liquid development. This high sensitivity to refractive index gradients makes it possible to identify the limit of the line of sight between the liquid fuel and the ambient gases [13]. The sensitivity is a function of the light intensity and is adjustable by a diaphragm in front of the camera; a smaller diaphragm opening increases the sensitivity. The scheme of the optical setup is presented (see Figure 1): two concave mirrors (f = 863.6 mm, d = 108 mm) are mounted in front of the optical windows of the chamber at 57 cm (see Figure 1, N°2) and 84 cm (see Figure 1, N°5). A 538 nm light beam from a LED (HardSoft DLR IL104G) passes through the concave mirror, crosses the chamber, and by means of another concave mirror passes through a diaphragm.

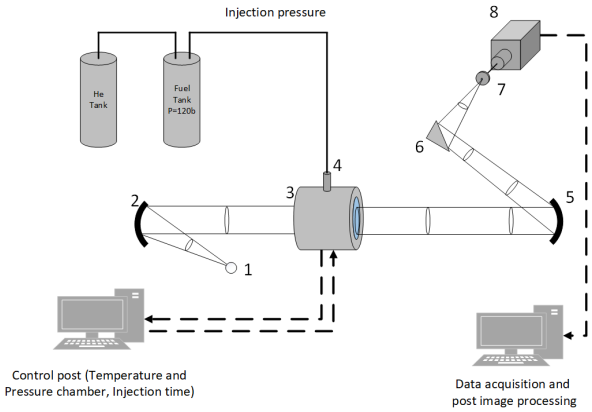

Figure 1. Scheme of the experimental and optical setup; 1 Light ED source; 2 and 5 Concave mirrors; 3 Chamber; 4 Injector; 6 Plane mirror; 7 Adjustable diaphragm; 8 CMos FastCam (High-speed camera).

The images are recorded at 15,000 frames per second with a Cmos high-speed camera (FastCam SA5, Photron), associated with a 105 mm Nikkon camera lens, to reach an image resolution of 768 × 648 pixels^2, with a spatial resolution of 0.160 mm/pixel. For each operating condition, 10 repetitions were done with 100 images recorded. Shutter time is set to 1/147000 second.

Image Post-Processing

The post-processing of 100 consecutive raw images is performed in several steps in a Matlab environment for each condition. The first six raw images were used to generate an average background. After subtraction of this average background and inversion, the image was binarized using Otsu's method for thresholding [14]. To simplify the calculation of spray penetration and the different angles, the binarized image was rotated. On the rotated image, spray penetration length (SP) and spray angle at 1/4 SP were calculated as displayed in Figure 2.

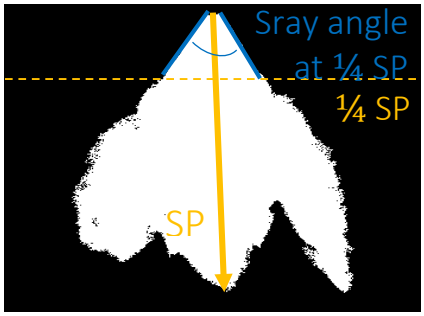

Figure 2. Definition of spray characteristics for the liquid spray of ethanol as an example

SP is the distance between the injector and the end of the spray. The spray angle at 1/4 SP is the value of the angle from the injector outlet to the quarter spray penetration length. Moreover, the area of the spray is measured by summing the white pixel of the binarized image.

Experimental Conditions

The experimental data presented in this study correspond to different conditions of ambient pressures, temperatures, and air densities summarized in Table 1. The injection pressure, P_{fuel}, was set at 120 bar and the injection temperature, T_{fuel}, was considered maintained at the ambient temperature, i.e 20°C, as there is no thermocouple in the injector nozzle. Two injection timings are set, the first at 4ms to characterize the spray morphology and the second at 1ms to evaluate the vaporization process. Four ratios of ammonia/ethanol (25%, 50%, 75%, and 90% of NH_3 by mole defined as X25, X50, X75, and X90) are compared to pure fuels. They are prepared in the liquid phase thanks to a mixing set-up using an emulsifier already used in [15].

Table 1. Experimental conditions for all fuel compositions.

Ambient Temperature [°C]	Ambient Pressure [Bar]	Air Density [kg/m^3]
20	2	2.38
	4	4.76
	7	8.32
80	2.41	2.38
	4.82	4.76
	8.43	8.32
120	2.69	2.38
	5.37	4.76
	9.39	8.32

Results and discussion

Spray characteristics

The phase state of the mixture is calculated with the equation of the state of Peng-Robison using the full methodology described in [16]. Figure 3 shows the calculation of the Vapor-Liquid Equilibrium (VLE) diagram for ammonia and ethanol. The calculated bubble and dew point curves are compared to the experimental conditions for the three temperatures investigated.

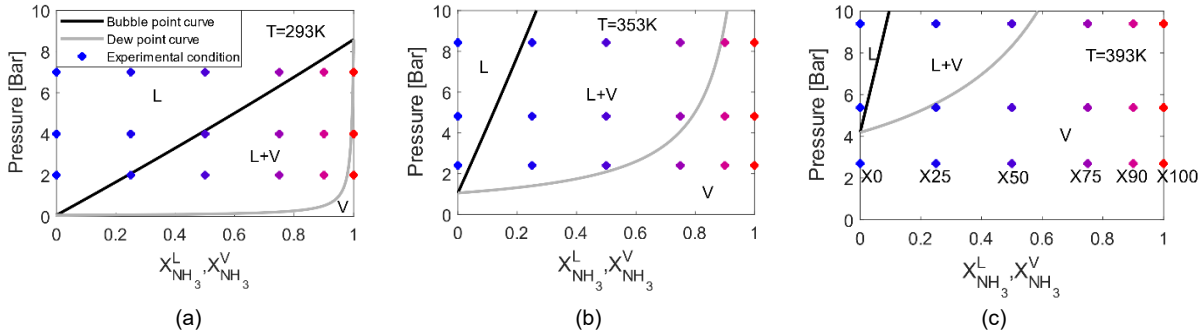

Figure 3. Vapor-Liquid Equilibrium calculation of ammonia/ethanol and experimental conditions for the three temperatures (a) 20°C (b) 80°C and (c) 120°C with the color range as a function of ammonia ratio

The color range corresponds to the ratio of ammonia in the blend: more the color is through the red, more the content of ammonia is important. As the temperature increases, the bubble and dew point curves change, and consequently the distribution of experimental conditions in each region of the diagram changes with temperature. As the temperature increases, the liquid region decreases, 7 conditions in the liquid phase at 293K down to 2 conditions at 393K. Conversely, the experimental conditions in the vapor state are only 3 at 293K and 14 at 393K. The ratio of the saturation pressure to the ambient pressure, commonly called Rp, is a classical criterion to identify the flash boiling condition for pure fuel; Rp>1 means flash boiling condition. However, for a binary fuel, the use of the LVE diagram is essential to identify the regions with or without flash boiling. The liquid phase means a “classic” vaporization while the addition of ammonia in ethanol will accelerate the vaporization due to their liquid+vapor position in the diagram. The vapor region means a flash boiling phenomenon during the injection process.

Figure 4 shows the raw spray images after 1 ms of injection for the different air densities, temperatures, and ratios of ammonia. Blue images represent liquid phases, grey images represent liquid and vapor phases and red images

represent vapor phases. For the low air density, the blue images (liquid) on the left, pure ethanol, and X25, are similar and some of the individual plumes are distinguishably meaning few interactions between them. These weak interactions are mainly due to the liquid state of these mixtures, as seen in Figure 3, thus meaning a slow vaporization process. On the contrary, for the red images which correspond to the vapor phase in Figure 3, the sprays are very thin and collapse with a strong plumes-to-plumes interaction. The individual plumes are not visible due to the rapid vaporization. This rapid state change decreases quickly the temperature inside the global spray creating a low-pressure region inside and the plumes get closer. Nevertheless, the spray on the red image for the pure ethanol at high temperature is less collapsed mainly due to the slower vaporization process of the ethanol compared to ammonia. Between these two opposite spray morphologies, the 'transient' spray morphologies are observed. For the ratio X50 at 20°C and X25 at 80°C, the individual plumes are not visible but the sprays are not collapsed as the spray is large. It can be explained by the fact that ammonia vaporizes at first but the decrease in the temperature inside the spray is not enough cold to collapse the spray. However, when more ammonia is added to the blend, X75 and X90 at 20°C, the spray collapses with a strong interaction between plumes probably due to a colder temperature inside the spray because of a higher amount of ammonia vaporized. For the low air density, the spray shapes are correlated to the liquid-vapor equilibrium calculation. For the high air density, no clear tendency as a function of the ammonia ratio can be underlined as the high pressure strongly affects the spray morphology.

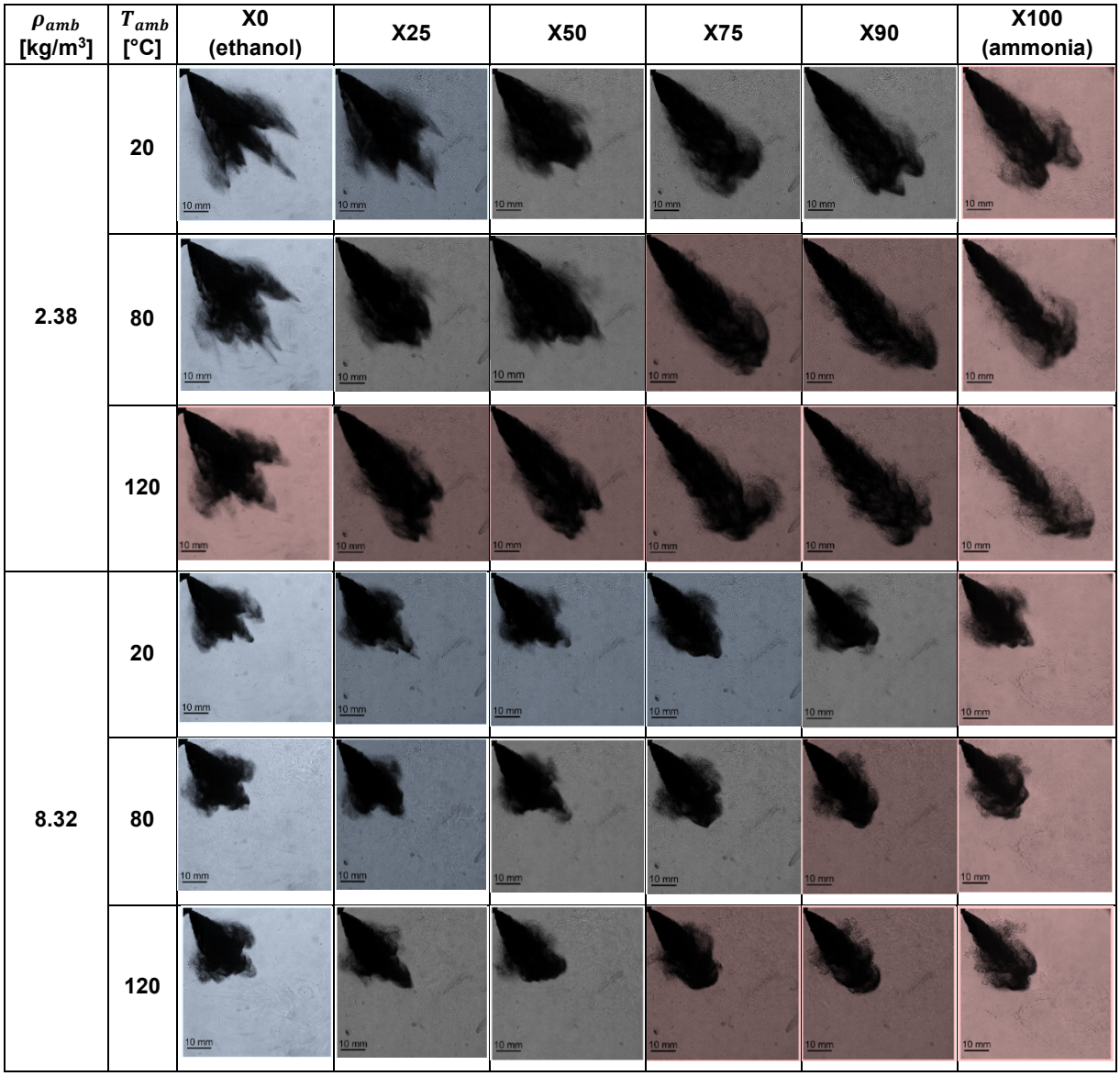

Figure 4. Comparison of spray shape at 1 ms after the start of injection obtained for the different ratios of ammonia, air densities, and temperatures, P_{in} =120bar. The color code corresponds to the phase state of VLE calculation: blue = liquid phase, red = vapor phase, and grey = liquid+vapor phase

Figure 5 shows the spray penetration with its standard deviation envelope for the different ammonia ratios and temperatures and air densities. In Figure 5.a and Figure 5.c, at low air density, two groups are observed before t=0.75ms and t=0.5ms respectively with two speeds of spray development. The first one regroups the sprays with an ammonia ratio below 50%, characterized by slow evaporation and weak plumes-to-plumes interactions. The second one regroups the spray with a higher ammonia ratio, characterized by a rapid change of phase state and with a strong collapsing effect. However, after t=0.75ms more differences are observed between the blends and the spray development is quicker when more ammonia is added. It can be explained by the collapsing effect that increases the spray penetration velocity. The low-pressure zone inside the spray due to the rapid vaporization brings the individual plumes together reducing the friction between the spray and the air. In Figure 5.b and Figure 5.d, at high air density, the spray penetrations are very close and only a few differences could be observable. Comparatively, to the low air density, spray developments are slower.

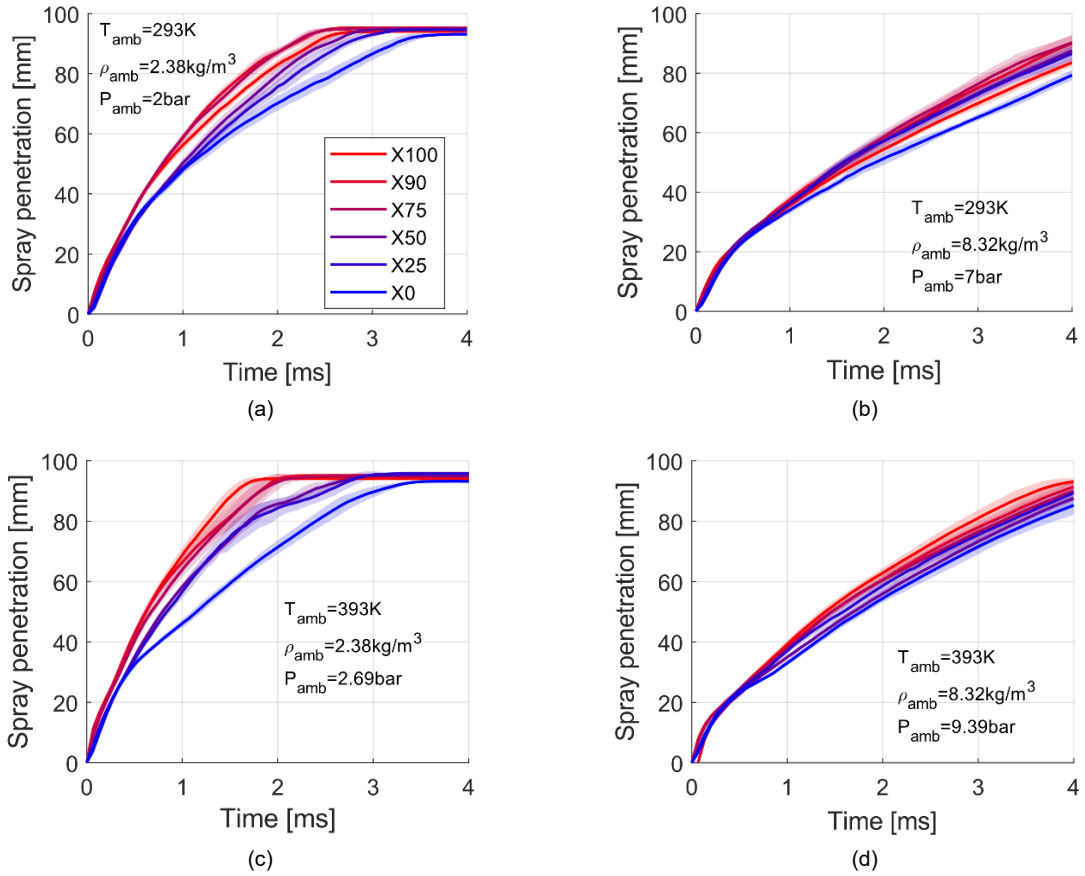

Figure 5. Spray penetration with its standard deviation envelope for the different ammonia ratios (a) at low density and low temperature, (b) at high density and low temperature, (c) at low density and high temperature, and (d) at high density and high temperature, P_{in} =120bar.

Figure 6 displays the spray angles with their standard deviation envelopes at the quarter of the spray penetration length. In Figure 6.a, at low air density and temperature, a similar angle is measured for all the ammonia ratios before t=0.75ms, nevertheless, after this duration, the two groups of ammonia ratios are formed. The spray angle of the first group (X0 to X50) is 45° while for the second group (X75 to X100), the spray angle is 35°. The sprays are thinner for the high ratio of ammonia due to the collapsing effect, as previously explained. However, with the increase of the air density, Figure 6.b, the spray angle evolutions get closer for all the ammonia ratios and reach 50°. At high temperature, Figure 6.a and 6.b, the spray angles are clearly sorted as a function of the ammonia ratio. Ethanol has a more opened angle (~50°) and then the angle decreases when ammonia is added down to 30°. This observation is mainly due to the collapse effect being more and more present due to a continuous decrease of the inner spray temperature when ammonia is added. By increasing the air density, Figure 6.d, the spray angle evolutions get closer and are a bit higher, 35° for the pure ammonia.

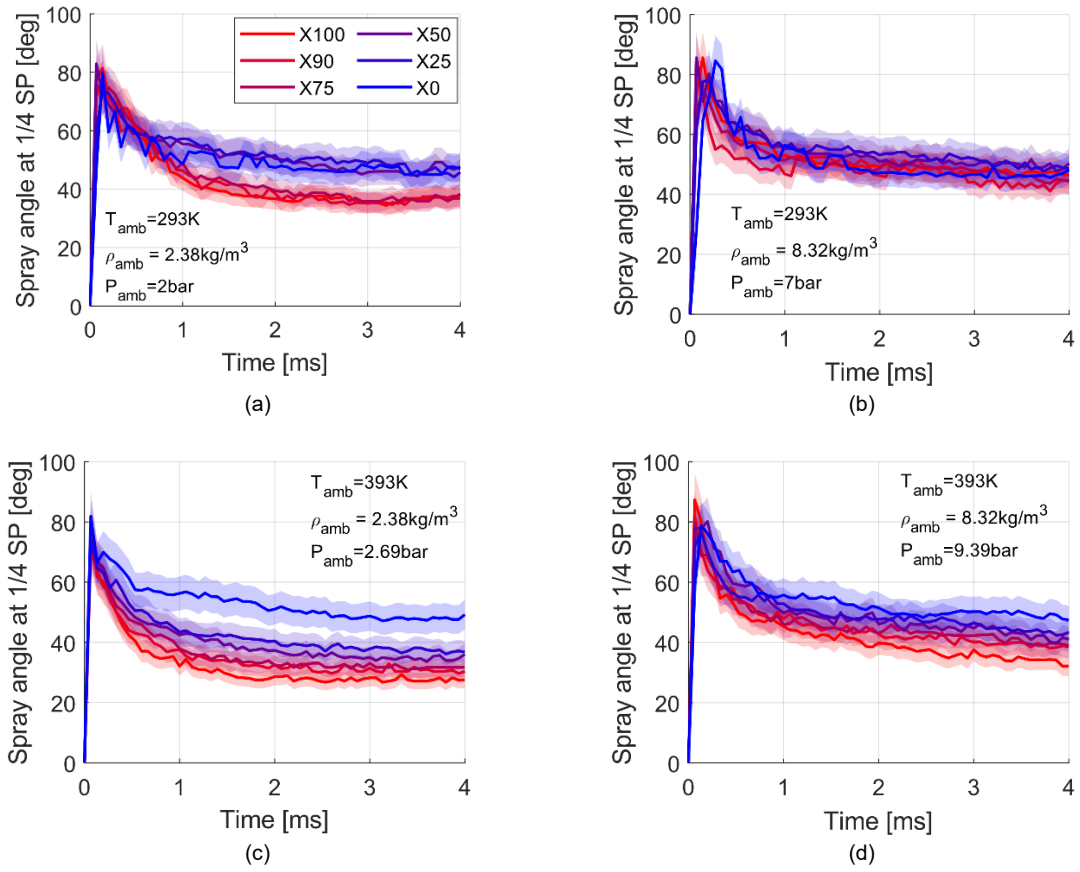

Figure 6. Spray angle with its standard deviation envelope at the quarter of the spray penetration for the different ratios of ammonia (a) at low density and low temperature, (b) at high density and low temperature, (c) at low density and high temperature, and (d) at high density and high temperature, P_{in} =120bar.

Vaporization process

To characterize the vaporization process, the injection duration was reduced to 1 ms and the recorded duration was increased up to 20ms to follow the area of the liquid spray even after the end of the injection timing. The raw data obtained are then normalized by the maximum area (at timing $t_{max\ area}$) and the time is adjusted between the timing where the area is maximum (set to 0 in Figure 7) and the end of the record (set to 20ms - $t_{max\ area}$ in Figure 7).

The results of the vaporization are presented in Figure 7. Pure ethanol is the slowest to vaporize in each condition. Figure 7.a, at low air density and temperature, the vaporizations of X0, X25, and X50 are very long and are not finished after 18ms while for the blends with high content of ammonia, they are totally vaporized in less than 10ms. Increasing the air density (Figure 7.b) increases the total vaporization duration. At a high temperature and low air density, Figure 6.c, the vaporization duration is drastically reduced. For all the conditions the vaporization durations are below 5ms and even below 2ms for pure ammonia and the difference between ammonia and ethanol is small. At high air density and temperature, the vaporization duration is increased and even more for the low ratio of ammonia. So clearly, the increase of the temperature and the addition of ammonia reduced the vaporization duration contrary to the increase of the air density. At least 50% of ammonia addition to ethanol is needed to strongly decreases the vaporization process.

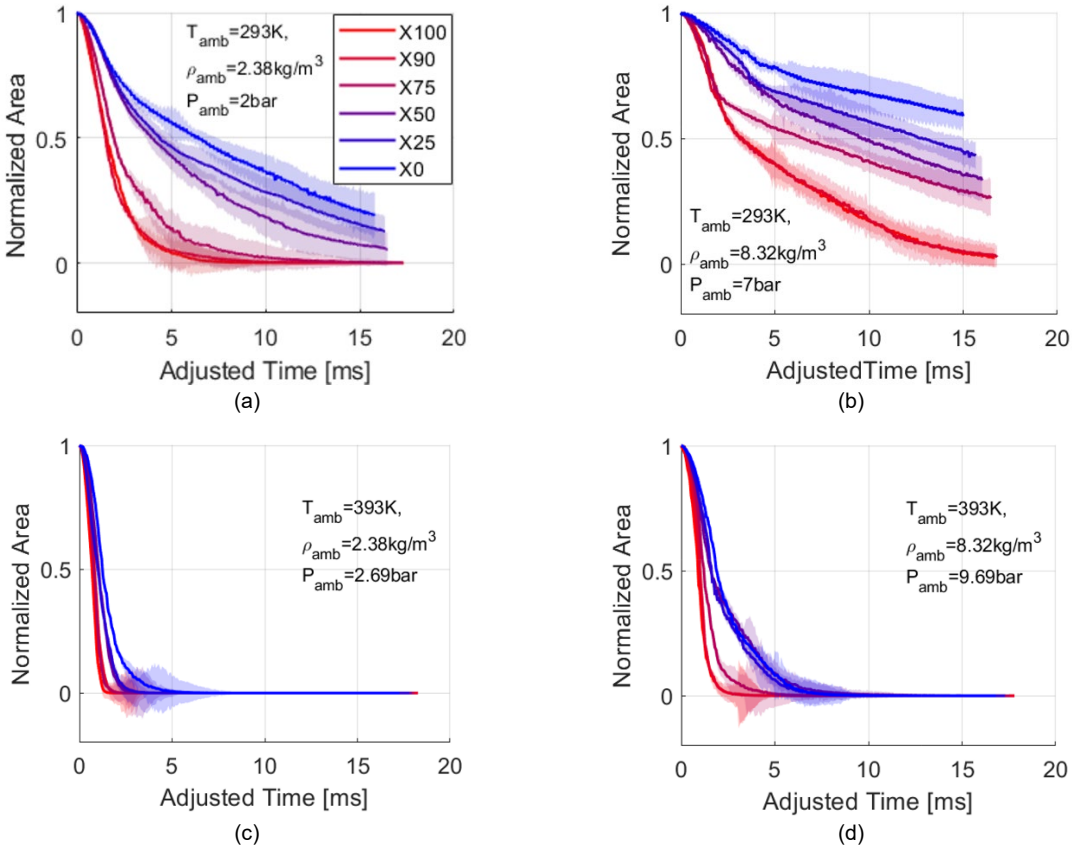

Figure 7. Evolution of the normalized area with its standard deviation envelope with an injection duration fixed at 1ms (a) at low density and low temperature, (b) at high density and low temperature, (c) at low density and high temperature, and (d) at high density and high temperature.

Droplet Vaporization

The droplet vaporizations in the same conditions of air density and temperature were estimated to complete this study and to better understand the process of multicomponent vaporization. The evaporation model used is from [17][18]:

$$\dot{m}_i = -2\pi D_i r_d \rho_{air} \, ln(1 + BM_i) \, Sh_i \quad (1)$$

Where $\dot{m}_i$, D_i, r_d, ρ_{air}, BM_i and Sh_i represent respectively the mass flow rate of the specie "i", the diffusion coefficient of the specie "i", the droplet radius, air density, the Spalding mass transfer number of the specie "i", and the Sherwood number of the specie "i".

In the case of flash boiling conditions, i.e. when the equilibrium pressure P_{eq} estimated by the Peng-Robinson equation is higher than the ambient pressure, the following model from [19] studying the evaporation of aqueous ammonia droplets was used. Moreover, Cai et al. [20] introduced a corrective factor, φ to take the mass diffusion in the droplet into account in the model:

$$\dot{m}_i = -2\pi r_d M_i D_i Sh_i \left(\frac{x_i^V P_{eq}}{RT_d} - \frac{x_i^\infty P_{amb}}{RT_{amb}} \right) \varphi \quad (2)$$

where x_i^V, x_i^∞ are the mole fraction in the vapor phase of the specie "i" calculated with the Peng-Robinson equation and the mole fraction far away from the droplet (in this study: $x_i^\infty = 0$), respectively. T_d is the droplet temperature.

The heat transfer is considered as followed:

$$mC_p \frac{dT_d}{dt} = h4\pi {r_d}^2 (T_{amb} - T_d) + \sum_{i=1}^{N} \Delta H_i^{Vap} \dot{m}_i \quad (3)$$

Where m is the droplet mass, C_p is the heat capacity of the droplet, h is the heat transfer coefficient and ΔH_i^{Vap} is the latent heat of the specie "i". The initial conditions of the droplet are: T_d=293K and r_d = 5µm. This radius corresponds to the measurement of some droplet size distribution as obtained in [21,22] for the same injector, ambient conditions, and injection pressure.

Figure 8 compares quantitively the experimental and numerical vaporization duration for the condition at high temperature because the sprays are totally vaporized, as already seen in Figure 7.c and 7.d. The same order of

duration magnitude was found between experimental and numerical data. Following this global agreement, a detailed analysis of droplet vaporization can therefore provide some information on global spray vaporization.

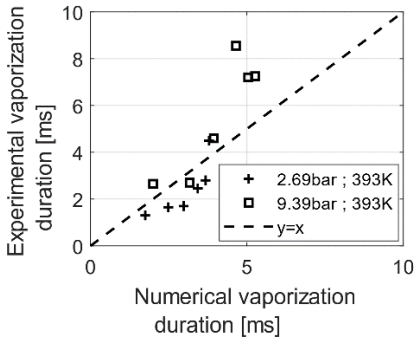

Figure 8. Comparison of the vaporization duration between the experimental and numerical data

Figure 9 shows the results of the calculation of the droplet vaporization under low air density and low temperature condition using equations (1)-(3). The mass, the temperature, and the ammonia fraction in the total mass vaporized of the droplet are displayed and the zoom at the start of the calculation enables to see the change of regime between the flash boiling and the vaporization.

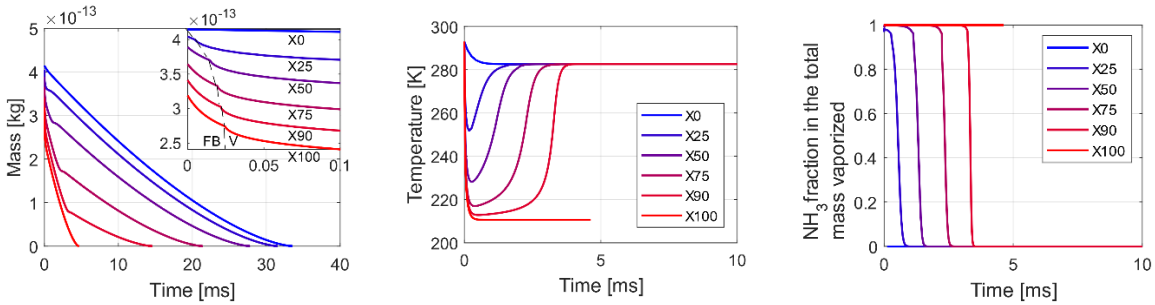

Figure 9. (a) Mass evolution with a zoom on flash boiling (FB) and the vaporization (V) models (b) the temperature evolution and (c) the ammonia fraction in the total mas vaporized of the droplets composed of different ammonia ratios and for T_{amb} =293K, ρ_{amb} =2.38kg/m^3 and P_{amb}=2bar

In Figure 9.a, the flash boiling mode is very short, less than 0.03ms and 14% of the mass is vaporized during this process for the pure ammonia condition. Regarding the temperature evolution, Figure 9.b, the flash boiling process corresponds to the major part of the temperature drop. Flash boiling is a very short but intense phenomenon. During the vaporization phase, in Figure 9.a, two trends of vaporization can be observed between the pure fuels with a slower rate of vaporization for ethanol compared to the pure ammonia. The total duration of evaporation is 7 times higher for ethanol (33.5ms) than for pure ammonia (4.6ms). The different vaporization rate is mainly explained by the difference in the diffusion coefficients: D_{NH_3}=0.1053.10^{-4} m^2/s and $D_{C_2H_5OH}$=0.0574.10^{-4} m^2/s, twice higher for ammonia. Regarding the blends, a breakpoint is present in their mass evolutions, indicating a change in the rate of vaporization. The cause of this change is highlighted in Figure 9.c, where ammonia first dominates the vaporization, and a similar rate of vaporization is observed at the beginning compared to pure ammonia. However, when all ammonia content is vaporized, only ethanol vaporizes, and the rate of evaporation “switches” to a similar rate of ethanol evaporation. Figure 9.b, shows the temperature evolution and the equilibrium temperature of ethanol is 282K (9°C) while pure ammonia is 210K (-63°C). This very low temperature is explained by the two different rates of vaporization but also by the difference in latent heat: 877 kJ.kg^{-1} and 1163 kJ.kg^{-1} for ethanol and ammonia respectively. For the blends, the temperature drops due to the ammonia vaporization and then increases to reach the equilibrium temperature of ethanol. It corresponds to the breakpoint seen previously in Figure 9.a and Figure 9.c. As more ammonia is added to the droplet, the temperature becomes colder and tends to reach the equilibrium temperature of ammonia. Moreover, the cold phase is longer when more ammonia is added. A high drop in temperature and long duration for the cold phase seem necessary conditions to collapse the spray.

Increasing the air density to ρ_{amb} =8.32kg/m^3 increases the vaporization duration, Figure 10.a, as experimentally observed because the rate of vaporization decreases due to a decrease of the Spalding number. Consequently, the drop in the temperature is a bit reduced, as visible in Figure 11, but still very cold for ammonia: 227K. For the low air density and high temperature, Figure 10.b, the vaporization durations are drastically reduced compared to the low temperature and air density, as shown in Figure 9.a, by a factor of 9 for pure ethanol and 3 for pure ammonia

due to a higher rate of vaporization. In terms of temperature, in Figure 11, ethanol gets heat and the droplet temperature increases up to 320K while for ammonia its temperature is still cold, 225K. This difference can be partially explained by the difference in the heat capacity between ammonia and ethanol. The heat capacity of ammonia is twice higher than ethanol meaning a higher “resistance” to increase the temperature. At high air density and high temperature, in Figure 10.c, the same tendencies are also observed, with an increase in the vaporization duration and the temperature compared to Figure 10.b for the same reasons as previously explained.

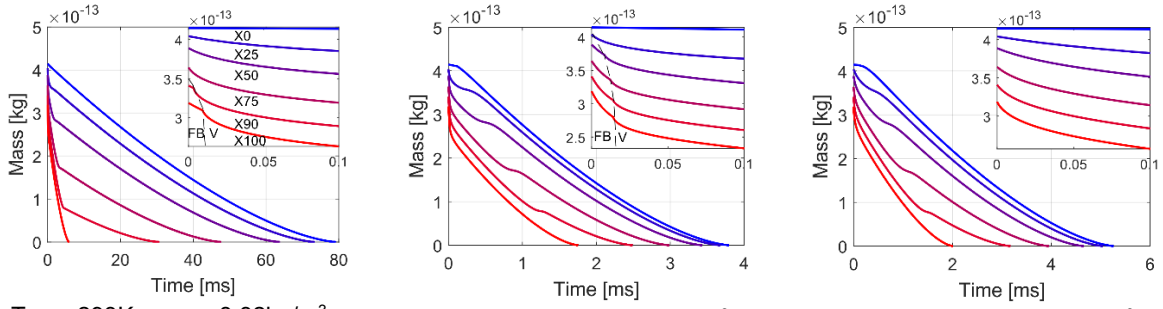

T_{amb} =293K ; ρ_{amb} =8.32kg/m^3 ; P_{amb}=7bar (a)

T_{amb} =393K ; ρ_{amb} =2.38kg/m^3 ; P_{amb}=2.69bar (b)

T_{amb} =393K ; ρ_{amb} =8.32kg/m^3 ; P_{amb}=9.39bar (c)

Figure 10. Mass evolution with a zoom on flash boiling (FB) and the vaporization (V) models of the droplets composed of different ammonia ratios and for different air density and temperature conditions

Moreover, to have a significant reduction in evaporation duration more than 50% of ammonia should be added to the blend as experimentally observed in Figure 7.

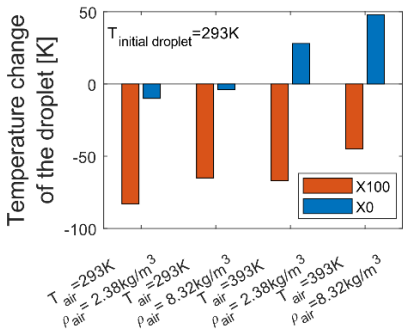

Figure 11. Comparison of the temperature change of the droplet between the ethanol and ammonia

Conclusions

The present study provides the first information on the spray characteristics and vaporization process of ammonia-ethanol blends with a current engine injector focusing on different conditions of air density and temperature.

From the Schlieren images and low air density, it was concluded that the spray shapes are correlated to the Liquid-Vapor equilibrium diagram. Sprays located in the liquid region in the diagram have similar weak plumes-to-plumes interactions due to slow vaporization and a liquid phase state. For the liquid-vapor region, a transient phase is observed. And when the vapor region is reached, plumes-to-plumes interaction is stronger with a collapsing effect due to a drop of the temperature inside the spray creating a low-pressure zone. However, at high air density, few differences were observed between the different fuel compositions.

Concerning the spray characteristics, the spray penetration increases when ammonia is added in the blend at low air density while for the high air density, no effect is observed; the spray angles become smaller when ammonia is added, and a difference up to 15° can be observed between pure ammonia and ethanol at high temperature and low air density.

It was pointed out that at least 50% of ammonia is needed to reduce significantly the vaporization process experimentally and numerically with droplet calculation.

The droplet vaporization estimation highlights similar results compared to the experimental data. At low air density and low temperature, the calculation indicated droplet temperature drop: from 9°C to -63°C from pure ethanol to pure ammonia, respectively. This low temperature is due to the higher energy of vaporization because of a higher diffusion coefficient for ammonia and higher heat of vaporization. The vaporization of the blends is firstly dominated by the vaporization of ammonia and then when all ammonia is vaporized, ethanol starts to vaporize.

An increase in air density tends to slow down the vaporization process due to a lower Spalding number decreasing the rate of vaporization and consequently reducing the drop of temperature or increasing the temperature of the

droplet. A temperature increase leads to a decrease in the vaporization duration. However, the droplet temperature of pure ammonia is still cold compared to ethanol due to their difference in heat capacity.

Acknowledgments

This work was supported by the French Government's "Investissement d'Avenir" program: "Laboratoire d'Excellence CAPRYSSES" (Grant No ANR-11- LABX-0006-01)

Nomenclature

$A(t)$	Spray area evolution [mm^2]
BM_i	Spalding number [-]
C_p	Heat capacity [J/K]
ΔH_i^{Vap}	Latent heat of vaporization [J/kg]
D_i	Diffusion coefficient [m^2/s]
h	Heat transfer [J/m^2/s/K]
m	Mass of the droplet [kg]
$\dot{m}_i$	Mass flow rate vaporization [kg/s]
M_i	Molar mass [g/mole]
P_{amb}	Ambient pressure [Pa]
P_{eq}	Equilibrium pressure of the binary mixture [Pa]
r_d	Droplet radius [m]
ρ_{air}	Air density [kg/ m^3]
φ	Corrective factor [-]
Sh_i	Sherwood number [-]
t	Time [s]
T_{amb}	Ambient temperature [K]
T_d	Droplet temperature [K]
X100	Blend with the ammonia ratio [-]
x_i^V	Mole fraction of "i" in the vapor phase [mole/mole]
x_i^∞	Mole fraction of "i" faraway of the droplet [mole/mole]

References

[1] C. Lhuillier, P. Brequigny, F. Contino, C. Mounaïm-Rousselle, Proc. Combust. Inst. 38 (2021) 6671–6678.
[2] C. Mounaim-Rousselle, P. Brequigny, Front. Mech. Eng. (2020).
[3] P. Dimitriou, R. Javaid, Int. J. Hydrogen Energy 45 (2020) 7098–7118.
[4] A.Z. Mendiburu, C.H. Lauermann, T.C. Hayashi, D.J. Mariños, R.B. Rodrigues da Costa, C.J.R. Coronado, J.J. Roberts, J.A. de Carvalho, Energy 257 (2022).
[5] A. Montanaro, L. Allocca, Combust. Sci. Technol. 191 (2019) 1600–1608.
[6] M. Xu, Y. Zhang, W. Zeng, G. Zhang, M. Zhang, SAE Int. J. Fuels Lubr. 6 (2013) 137–148.
[7] M. Chang, Z. Lee, S. Park, S. Park, Fuel 271 (2020) 117600.
[8] J.D. Naber, D.L. Siebers, SAE Tech. Pap. (1996).
[9] M. Chang, J. Hwan Park, H. Ik Kim, S. Park, Appl. Therm. Eng. 170 (2020) 114969.
[10] R. Pelé, C. Mounaïm-Rousselle, P. Bréquigny, C. Hespel, J. Bellettre, Fuels 2 (2021) 253–271.
[11] E. Tinon, Etude Expérimentale Des Mécanismes d'atomisation Effervescente. Application à La Sécurité Incendie Dans Les Moteurs Aéronautiques, UNIVERSITÉ DE TOULOUSE, 2018.
[12] J. Dernotte, (2012) 261.
[13] J. Pastor, R. Payri, J. Garcia-Oliver, J. Nerva, in: SAE Tech. Pap., 2012.
[14] N. Otsu, IEEE Trans. Syst. Man, Cybern. 9 (1979) 62–66.
[15] Y. Ji, J. Bellettre, A. Montillet, P. Massoli, Int. J. Multiph. Flow 131 (2020) 103402.
[16] R. Privat, J.N. Jaubert, Y. Privat, Comput. Chem. Eng. 50 (2013) 139–151.
[17] S.S. Sazhin, A. Elwardany, P.A. Krutitskii, G. Castanet, F. Lemoine, E.M. Sazhina, M.R. Heikal, Int. J. Heat Mass Transf. 53 (2010) 4495–4505.
[18] Z. Ni, C. Hespel, K. Han, F. Foucher, Int. J. Heat Mass Transf. 164 (2021).
[19] T. Eldredge, M. Thomas, Am. Soc. Mech. Eng. Power Div. POWER 1 (2018) 1–7.
[20] B. Cai, Q. Wang, S. Yin, H. Gu, H. Wang, H. Zhen, L. Zhang, Appl. Therm. Eng. 148 (2019) 704–713.
[21] J. Zembi, M. Battistoni, A. Pandal, C. Rouselle, R. Pelé, P. Brequigny, C. Hespel, in: SAE Tech. Pap., 2023, pp. 1–20.
[22] J. Zembi, M. Battistoni, A. Pandal, C. Rouselle, R. Pelé, P. Brequigny, C. Hespel, J. Ammon. Energy (2023) 1–9.